Earth Planet. Sci. Lett. 666 (2025) 119498

Contents lists available at ScienceDirect

Earth and Planetary Science Letters

journal homepage: www.elsevier.com/locate/epsl

Controls on uranium isotope fractionation in the late Paleoproterozoic ocean

Alexandra Kunert [a,*], Simon W. Poulton [b], Donald E. Canfield [c], Philip W. Fralick [d], Geoffrey J. Gilleaudeau [e], Brian Kendall [a]

[a] Department of Earth and Environmental Sciences, University of Waterloo, Waterloo N2L 3G1, Canada
[b] School of Earth and Environment, University of Leeds, Leeds LS2 9JT, United Kingdom
[c] Nordcee and Institute of Biology, University of Southern Denmark, Odense 5230, Denmark
[d] Department of Geology, Lakehead University, Thunder Bay P7B 5E1, Canada
[e] Department of Atmospheric, Oceanic and Earth Sciences, George Mason University, Fairfax 22030, United States

ARTICLE INFO

Edited by: Dr Tristan Horner

Keywords:
U isotopes
Black shale
Proterozoic oceans
Ocean redox
Ocean productivity

ABSTRACT

Uranium isotope data from Proterozoic carbonates ($\delta^{238}U_{carb}$) and black shales ($\delta^{238}U_{auth}$) are enigmatic. Average Proterozoic $\delta^{238}U_{carb}$ (approximating Proterozoic seawater, $\delta^{238}U_{sw}$) is similar to modern river/seawater $\delta^{238}U$, and Proterozoic black shales do not always record highly fractionated $\delta^{238}U_{auth}$ compared to contemporaneous $\delta^{238}U_{carb}$. However, very light $\delta^{238}U_{carb}$ and heavy $\delta^{238}U_{auth}$ for the widely anoxic Proterozoic oceans was expected because large isotope fractionations accompany U reduction in anoxic environments. To address this enigma, we report black shale $\delta^{238}U_{auth}$ through a well-characterised multi-core transect in the late Paleoproterozoic Animikie Basin, North America. There is a wide range of $\delta^{238}U_{auth}$, from –0.52‰ to 0.53‰, that generally correlates with organic carbon enrichments. Heavy $\delta^{238}U_{auth}$ in organic-rich shallow shelf sediments within and near a euxinic wedge are attributed to enhanced productivity with vigorous sediment microbial activity, neutrally charged aqueous U species that slow reaction kinetics, and redoxcline fluctuations. In less organic-rich sediments of the anoxic-ferruginous deep shelf environment, characterized by lower productivity and plentiful reduced iron availability, light $\delta^{238}U_{auth}$ may reflect rapid U reduction or adsorption to solid Fe/Mn species. Hence, for the widely anoxic Proterozoic oceans, we propose that large isotopic fractionations (0.4 to 1.2‰) were associated with highly productive areas on anoxic continental margins, and muted isotopic fractionations (–0.1 to 0.4‰) occurred in anoxic deep-ocean environments. Low-productivity Proterozoic oceans yielded sediments with $\delta^{238}U_{carb}$ and $\delta^{238}U_{auth}$ close to modern river/seawater values, whereas higher-productivity basins (e.g., Animikie Basin) resulted in lower $\delta^{238}U_{carb}$ and more variable $\delta^{238}U_{auth}$.

1. Introduction

Uranium isotope compositions ($\delta^{238}U$) in carbonates and black shales are frequently used to reconstruct ancient global ocean redox conditions. This is done following a seawater mass balance approach built on U isotope systematics in the modern, well-oxygenated oceans (Asael et al., 2013; Cheng et al., 2020; Clarkson et al., 2023; Dang et al., 2022; Gilleaudeau et al., 2019; Kipp and Tissot, 2022; Lu et al., 2023, 2020; Stockey et al., 2020; Wang et al., 2018; Yang et al., 2017; Zhang et al., 2022). A tenet of the oceanic U isotopic mass balance is that seawater $\delta^{238}U$ ($\delta^{238}U_{sw}$) is controlled primarily by U removal from the oceans during reduction of U(VI) to U(IV) into sediments under anoxic (O_2-free) and/or euxinic (anoxic and sulfidic) water columns. Reduction induces an isotopic offset through preferential removal of ^{238}U into solid phases by a nuclear volume effect (NVE), compared to ^{235}U which preferentially remains in solution. As reduction often occurs within the sediment column, there may be an opposing diffusive isotope fractionation that halves the intrinsic NVE fractionation factor (Andersen et al., 2014). At times when limited U is removed to sediments under anoxic or euxinic bottom waters in otherwise well-oxygenated oceans, $\delta^{238}U_{sw}$ should approach the average riverine input $\delta^{238}U$ ($\delta^{238}U_{riv}$) of –0.29 ± 0.03‰, which is unfractionated from the upper continental crust at –0.29 ± 0.06‰ (Andersen et al., 2016; Tissot and Dauphas, 2015). This concept is illustrated by the modern ocean, whose homogenous global

* Corresponding author.
E-mail address: akunert@uwaterloo.ca (A. Kunert).

https://doi.org/10.1016/j.epsl.2025.119498
Received 28 October 2024; Received in revised form 9 April 2025; Accepted 8 June 2025
Available online 18 June 2025

$\delta^{238}U_{sw}$ of –0.38 ± 0.02‰ (Kipp et al., 2022) is only slightly lighter than average $\delta^{238}U_{riv}$, reflecting small areas of intense seafloor U reduction confined to silled basins (e.g., Black Sea, Cariaco Basin; Brüske et al., 2020b; Rolison et al., 2017), highly productive continental margin upwelling zones (e.g., Peruvian margin; Bruggmann et al., 2022; Cole et al., 2020), and permanently or intermittently anoxic fjords (e.g., Framvaren Fjord, Saanich Inlet; Holmden et al., 2015; Todd et al., 1988), as well as moderate U reduction in low-oxygen environments where O_2 penetration into sediments is < 1 cm (e.g., Senegal and Washington State margins; Morford and Emerson, 1999).

The U isotope paleoredox proxy has been used to infer the extent of anoxic seafloor during many Phanerozoic intervals, including oceanic anoxic events that experienced shifts to lighter than modern $\delta^{238}U_{sw}$ linked to expanded anoxic seafloor areas (e.g., Cheng et al., 2020; Dahl et al., 2014; Kulenguski et al., 2023). This approach is reasonable when the oceanic U residence time is long relative to ocean mixing times, thus enabling the U isotope proxy to capture global redox conditions. However, application of U isotopes as a global ocean paleoredox proxy to the less extensively oxygenated Proterozoic oceans may potentially be impacted by a lower oceanic U residence time compared to Phanerozoic oceans (Chen et al., 2021).

The goal in the application of the U isotope ocean mass balance is to estimate global U fluxes to, or areal extent of, discrete marine redox environments. The primary assumptions are that: $\delta^{238}U_{sw}$ is homogeneous in the global oceans, $\delta^{238}U_{riv}$ inputs are invariant and similar to modern, each redox environment features a distinct range of U isotope offsets ($\Delta^{238}U_{sed\text{-}sw}$) between authigenic sedimentary phases ($\delta^{238}U_{auth}$) and $\delta^{238}U_{sw}$, and the proportion of U transferred to each sink controls global $\delta^{238}U_{sw}$. Based on modern analogs, the sediment sinks have previously been defined by increasing isotopic offsets as marine redox conditions intensify from oxic ($\Delta^{238}U_{oxic\text{-}sw}$ = –0.2‰ to 0.05‰), through low-oxygen (O_2 < 90 μM; e.g., dysoxic, suboxic; $\Delta^{238}U_{lowO2\text{-}sw}$ = –0.05‰ to 0.1‰), ferruginous (Fe^{2+}-containing)/non-sulfidic anoxic ($\Delta^{238}U_{anoxic\text{-}sw}$ = –0.3‰ to 0.4‰), to euxinic ($\Delta^{238}U_{euxinic\text{-}sw}$ = 0.4 to 0.8‰, up to 1.2‰) (Bruggmann et al., 2022; Cole et al., 2020; Gilleaudeau et al., 2025, 2019; Rolison et al., 2017; Stockey et al., 2020; Wang et al., 2016; Yang et al., 2017; Zhang et al., 2022). However, these observations demonstrate significant overlap between modern oxic, low-oxygen, and non-sulfidic/ferruginous anoxic settings. There is evidence from black shales that ferruginous and euxinic settings can show overlapping U isotopic fractionation from 0.2 to 1.3‰ (Lau et al., 2022; Rutledge et al., 2024). Additionally, very large U isotope fractionations approaching the intrinsic isotopic fractionation factor of 1.2‰ have been observed in temporally dynamic, low oxygen to anoxic environments, and in weakly or moderately euxinic settings (Andersen et al., 2014; Clarkson et al., 2023). Such large isotopic fractionations may be attributed to partial U removal when reduction rates are low, or when reduction occurs near the sediment–water interface, within the water column or within a highly permeable organic floc (Andersen et al., 2014; Clarkson et al., 2023). The latter of these reduction scenarios is associated with minimal or no U diffusion through the sediment column (non-diffusion-limited conditions), and thus diffusive isotope fractionation (porewater ^{238}U depletion with sediment depth) does not counteract reductive isotope fractionation (^{238}U enrichment in sediment phases) (Andersen et al., 2014).

These observations contrast with assumptions that increasingly reducing environments scale with increased isotopic fractionations between seawater and sediments, complicating the interpretation of redox-based sediment sink areas using conventional mass balance models. Other environmental factors likely affect observed $\Delta^{238}U_{sed\text{-}sw}$, including chemical parameters such as aqueous U speciation, microbially mediated reduction, reaction kinetics, and organic matter burial rate (Brown et al., 2018; Lau et al., 2022, 2020; Rolison et al., 2017; Rutledge et al., 2024; Stylo et al., 2015). Physico-hydrographic factors, including sedimentation rate and basin restriction, may also impact isotopic fractionation (Lau et al., 2022, 2020; Rolison et al., 2017).

Carbonate $\delta^{238}U$ ($\delta^{238}U_{carb}$)—which may closely approximate $\delta^{238}U_{sw}$ if unaltered by diagenesis or metamorphism (Chen et al., 2018, 2016; Romaniello et al., 2013)—demonstrates a variable, but modern-like average of –0.40 ± 0.27‰ (1σ) from the late Paleoproterozoic to the early Neoproterozoic (~2060–800 million years ago, Ma) (Chen et al., 2021; Gilleaudeau et al., 2019). However, some intervals host lighter $\delta^{238}U_{carb}$ than average, e.g., the ~1850 Ma Duck Creek Dolomite (–0.75 ± 0.06‰) and ~1000–800 Ma Huaibei Group (–0.71 ± 0.23‰) (Gilleaudeau et al., 2019; Zhang et al., 2022). In addition, average authigenic $\delta^{238}U$ ($\delta^{238}U_{auth}$) values in Proterozoic black shales do not always demonstrate large isotopic fractionations compared to $\delta^{238}U_{carb}$ (Chen et al., 2021). Modern-like average Proterozoic $\delta^{238}U_{carb}$ could suggest well-oxygenated oceans, while limited isotopic offset between carbonates and black shales could point to non-uniformitarian/alternative control(s) on $\delta^{238}U_{sw}$ (Chen et al., 2021). Most evidence points to widespread deep-ocean anoxia in Proterozoic oceans (Partin et al., 2013; Poulton et al., 2010, 2004; Reinhard et al., 2013; Scott et al., 2008; Sheen et al., 2018), therefore the latter scenario is more likely to have affected Proterozoic $\delta^{238}U_{sw}$. Diagenesis may also have affected reported $\delta^{238}U_{carb}$ values, possibly shifting them heavier by up to ~0.3‰ (Chen et al., 2018), which is accounted for in $\delta^{238}U_{carb}$ compilations that estimate mid-Proterozoic $\delta^{238}U_{sw}$ in the range of –0.73‰ to –0.43‰ (Gilleaudeau et al., 2019).

A better understanding of marine U isotope systematics in the Proterozoic is necessary to reconcile modern-like $\delta^{238}U_{sw}$ in oceans that were likely widely anoxic. The Animikie Basin (Lake Superior region, North America) comprises a minimally metamorphosed sequence of iron formation (IF) and fine-grained siliciclastics deposited along a continental margin on the southwestern edge of the Superior Province (Johnston et al., 2006; Kendall et al., 2011; Poulton et al., 2010, 2004). Multiple drill cores containing ferruginous and euxinic black shales of the 1836 Ma Rove and Virginia formations enable a glimpse into U isotope systematics across a Paleoproterozoic shallow to deep shelf setting. The variable depositional and redox localities allow for an investigation of local U isotope fractionation mechanisms to provide a basis for evaluating mid-Proterozoic U isotope systematics.

2. Geological background

The Animikie Basin, located northwest of Lake Superior across the Ontario–Minnesota border, hosts late Paleoproterozoic IFs and black shales (Lucente and Morey, 1983) (Fig. 1). In Ontario, this includes the Gunflint Formation, which is dominated by IF, overlain by interbedded turbidites and organic-rich black shales of the Rove Formation (Lucente and Morey, 1983; Ojakangas et al., 2001) (Fig. 2). Correlative units of the Biwabik and Virginia formations, respectively, lie to the south in Minnesota, laterally separated from their Ontario counterparts by the ~1100 Ma mafic intrusive Duluth Complex (Lucente and Morey, 1983; Ojakangas et al., 2001). The succession was deposited along the coast of the supercontinent Nuna, on a continental margin undergoing extension during IF deposition (Fralick et al., 2002; Hemming et al., 1995; Pufahl and Fralick, 2004), which was transformed into a foreland basin with sediment derived from the uprising Trans-Hudson Orogeny to the northwest supplying the overlying shales and turbidites (see Supplementary Material for further discussion of Animikie Basin tectonic settings).

Uranium–lead zircon ages provide depositional constraints for Animikie Basin units. Tuffs in the middle Gunflint Formation give an age of 1878 ± 1 Ma (Fralick et al., 2002). Distal ejecta from the 1850 ± 1 Ma (Krogh et al., 1984) Sudbury Impact Event overlie ~2 m of limestone forming the upper member of the Gunflint Formation, and exhibit evidence of sub-aerial diagenesis (Fralick et al., 2017). Younger ages, between 1836 ± 5 Ma and 1832 ± 3 Ma, have been reported from ash bed zircons ~5 m above the Gunflint–Rove and Biwabik–Virginia contacts (Addison et al., 2005).

Metamorphism of these sedimentary sequences is typically sub-

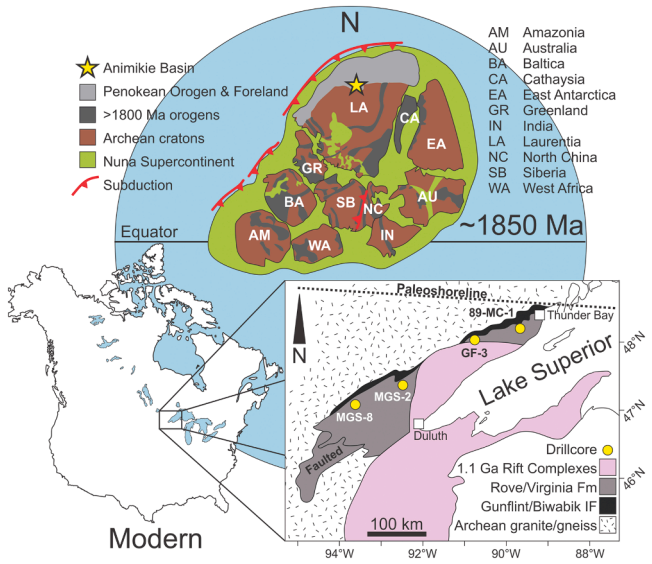

Fig. 1. Paleogeography of the supercontinent Nuna at ~1850 Ma (Zhang et al., 2012) showing the Animikie Basin along the northern continental coast, and modern location of the Animikie Group preserved in central North America (Poulton et al., 2010). Paleogeographic configuration and age is approximate as Zhang et al. (2012) mapped ~1740 Ma.

greenschist in Ontario to greenschist facies in northern Minnesota (Easton, 2000). Thus, the primary sedimentary geochemical and $\delta^{238}U$ signal is likely retained, since thermal maturation appears to have no impact on $\delta^{238}U$ values in black shales (Dickson et al., 2022). Higher grade hornfels facies occurs within ~1.5 km from the Duluth Complex (Labotka et al., 1981; Ripley et al., 2001). The GF-3 core underlies the northern edge of the Duluth Complex, with the contact occurring above our sample interval (>300 m above the Gunflint–Rove contact). Uranium systematics in the sampled portion do not appear to have been affected by contact metamorphism based on constant U_{EF} and $\delta^{238}U$ up-core (see Results).

Iron (Fe) speciation in the Animikie Basin has revealed that, following IF deposition from a ferruginous basin with mildly oxygenated surface waters, the basin transitioned to a more complex redox-stratified regime, with ferruginous deeper waters, euxinic intermediate depths, and oxygenated shallow waters (Poulton et al., 2010, 2004). Stratigraphic variability in these Fe speciation data suggests a landward migration of euxinia during sea level transgression. The geometry of the euxinic waters within the basin may have been similar to that of a modern oxygen minimum zone (OMZ), but with H_2S build-up starting at the sediment–water interface, where a large amount of organic matter was deposited and the sulfate influx from continental weathering was relatively high. The H_2S-rich waters formed a euxinic 'wedge' structure (as observed in modern OMZs; cf. Pizarro-Koch et al., 2023; Poulton et al., 2010), which created a barrier to upwelling Fe^{2+}-rich waters (Poulton et al., 2010, 2004). This redox structure may have been pervasive on other continental margins and could have been a mechanism that contributed to the cessation of IF deposition at this time (Kendall et al., 2011; Poulton et al., 2010, 2004).

No $\delta^{238}U_{auth}$ data have been reported from similarly aged black shales. However, the 1980 Ma Zaonega Formation and 1730 Ma Wollogorang Formation (Mänd et al., 2020; Yang et al., 2017) record U reduction and isotope fractionation, as $\delta^{238}U_{auth}$ is consistently heavier than modern $\delta^{238}U_{riv}$ (Zaonega: –0.03‰ to 0.79‰; less hydrothermally-altered samples from the Wollogorang: –0.17‰ to 0.00‰). Six samples from the Biwabik IF have $\delta^{238}U$ ranging from –0.63‰ to –0.19‰, and these light isotopic compositions and low U concentrations (< 0.97 μg g^{-1}) may reflect U(VI) adsorption to Fe (oxyhydr)oxides or reduction by Fe(II) with limited isotope fractionation (Wang et al., 2018).

3. Materials and methods

Black shale samples from the Rove and Virginia formations were obtained from four cores (89-MC-1, GF-3, MGS-2, MGS-8) deposited across a bathymetric transect in the Animikie Basin (Fig. 1), which were analysed for Fe-S-C systematics by Poulton et al. (2004, 2010). Fine-grained, organic-rich argillite of the lower Rove Formation in 89-MC-1 and GF-3 (inner shelf) and the Virginia Formation in MGS-2

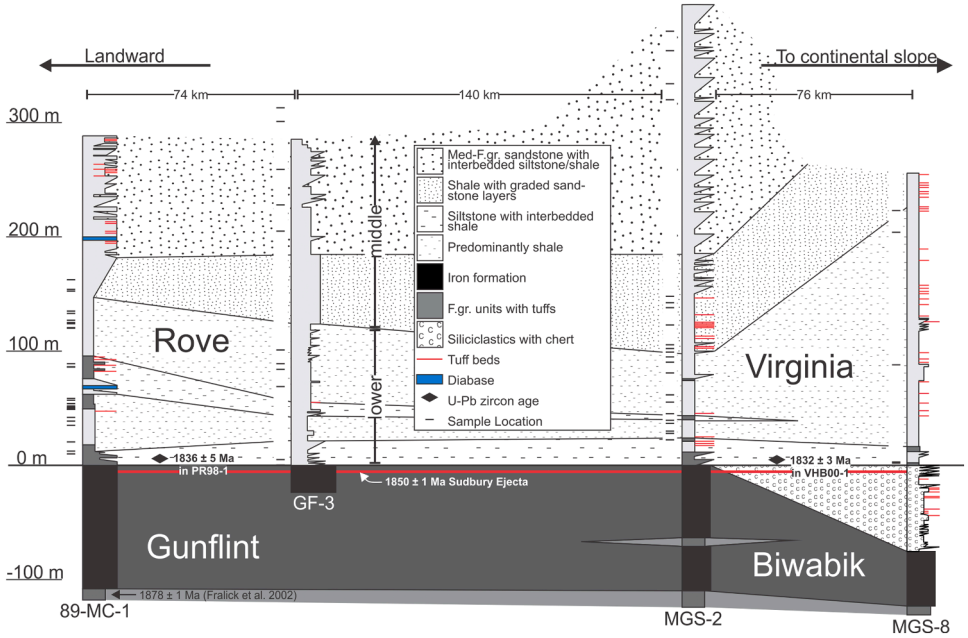

Fig. 2. Lithological cross section of Animikie Basin cores modified from Poulton et al. (2010). U-Pb zircon ages from cores PR98-1 and VHB00-1 (profiles not shown) from Addison et al. (2005). Sudbury ejecta age from Krogh et al. (1984). Cores 89-MC-1 and GF-3 contain Rove and Gunflint formations; MGS-2 and MGS-8 contain Virginia and Biwabik formations.

and MGS-8 (middle to outer shelf) (Fig. 2) suggest deposition in a quiet offshore environment during transgression onto the continental shelf when sediment supply was limited (Maric, 2006). The middle Rove/-Virginia formations feature coarser argillite with interbedded fine-/-medium-grained sandstones, indicating enhanced sediment supply and/or basin shallowing (Maric, 2006). Sampling focused on the lower Rove/Virginia formations, although several samples from the middle Rove/Virginia formations in GF-3 and MGS-2 were also analysed. Splits were processed at the Metal Isotope Geochemistry Laboratory (University of Waterloo) for multi-element compositions and $\delta^{238}U$.

3.1. Sample digestion and multi-element analysis

Ashed sample powders (550°C) were digested using trace-metal grade nitric, hydrochloric, and hydrofluoric acids. Core GF-3 required additional steps due to incomplete dissolution by this method—see Supplementary Material. Elemental concentrations were measured on an Agilent 8800 triple-quadrupole inductively coupled plasma mass spectrometer (ICP-MS). Several USGS black shale standards (SBC-1, SDO-1, SGR-1b) were digested and analysed alongside samples to verify method accuracy. Blank contents of elements included in this study were typically < 1%; U blank levels were always < 0.02% of the total U in a sample. Instrument precision was typically better than 5%. Procedural replicates for 13 samples were always within 5% difference.

3.2. Uranium isotope purification and analysis

Chemical separation of U from matrix elements was completed via anion exchange chromatography on UTEVA resin following the procedure described in Weyer et al. (2008). Purified U samples (100 ng g^{-1} U), double-spiked with isotopic reference material IRMM-3636a ^{233}U–^{236}U, were analysed on a Nu Plasma II multi-collector ICP-MS in dry plasma mode to determine isotopic compositions. Standard–sample bracketing against a double-spiked uranyl nitrate primary standard CRM-145 was used to normalize isotopic data by the delta notation ($\delta^{238}U$, Eq. 1) and monitor instrument drift.

$$\delta^{238}U\ (‰) = \left(\frac{^{238}U/^{235}U_{sample}}{^{238}U/^{235}U_{CRM145}} - 1\right) \times 1000 \quad (1)$$

Repeated measurements of CRM-145 ($\delta^{238}U_{CRM\text{-}145} = 0.00 \pm 0.09‰$; 2σ, $n = 208$) and double-spiked uranium oxide standard CRM-129a ($\delta^{238}U_{CRM\text{-}129a} = -1.43 \pm 0.13‰$; 2σ, $n = 79$) were used to verify instrument reproducibility. Our $\delta^{238}U_{CRM\text{-}129a}$ value is similar to previous measurements of this standard on the same Nu Plasma II (–1.42 ± 0.09‰, Lu et al., 2023; –1.42 ± 0.08‰, Yang et al., 2023). The USGS black shale standards SBC-1 (–0.26 ± 0.16‰), SDO-1 (–0.12 ± 0.07‰) and SGR-1b (–0.24 ± 0.15‰) prepared and analysed alongside samples were comparable to previously reported values, including those from other labs (Bruggmann et al., 2022; Chen et al., 2021; Lu et al., 2023, 2020; Rolison et al., 2017; Yang et al., 2023, 2017). Twelve full procedural replicates yielded uncertainties of < 0.08‰ (2σ on replicate means), except for GF-3-11 at ±0.16‰.

4. Results

4.1. Elemental compositions

To compare within and between cores, elemental concentrations are converted to enrichment factors (X_{EF}; Eq. 2) to normalize for varying detrital compositions:

$$X_{EF} = \frac{(X/Al)_{sample}}{(X/Al)_{UCC}} \quad (2)$$

where X is the element concentration, Al is aluminium concentration, and UCC is the upper continental crust composition (Mclennan, 2001). The redox sensitive trace metals (RSTMs) U, Mo, Re and V are generally enriched above the modern UCC ($X_{EF} > 1$) in all four cores (Fig. 3, Supplementary Data). Shallower cores (89-MC-1, GF-3) have generally larger metal enrichments than deeper cores (MGS-2, MGS-8). Compositional variation is significantly greater within 89-MC-1 and MGS-2, which is consistent with Fe speciation analyses (Poulton et al., 2010, 2004), and RSTM contents align with the redox zonation ascribed from those studies, supporting a robust redox signal.

In euxinic intervals identified by Fe speciation (Poulton et al., 2004, 2010), RSTMs commonly show larger enrichments compared to ferruginous samples, although in core 89-MC-1 there is considerable overlap (see Fig. 3), possibly reflecting RSTM drawdown due to the development of sulfidic porewater conditions close to the sediment–water interface (supported by a relatively high degree of pyritization for these samples; Poulton et al., 2010). For a few samples (5 in core 89-MC-1) with equivocal Fe speciation, we take the common approach of utilizing RSTMs to reconstruct water column redox conditions. Three of these samples have elevated RSTM EF values, supporting anoxic depositional conditions, and since the Fe speciation data for these samples do not indicate euxinic deposition, we characterise them as being deposited under ferruginous conditions. The remaining two samples have relatively low Re_{EF}, Mo_{EF} and V_{EF} values, with distinctly lighter U isotope signatures (Fig. 3), and may therefore have been deposited under low-oxygen conditions, rather than full anoxia. We note that low metal EFs and light $\delta^{238}U$ may alternatively indicate intermittent basin restriction that led to water column metal depletion and an isotope reservoir overwhelmed by the local riverine supply.

4.2. Authigenic uranium isotope compositions

The Rove and Virginia black shales encompass a wide range of bulk sediment $\delta^{238}U$ ($\delta^{238}U_{bulk}$), from –0.45‰ to 0.43‰ (Supplementary Data). To correct for detrital influence, $\delta^{238}U_{bulk}$ is converted to an authigenic composition ($\delta^{238}U_{auth}$) using Eq. 3, which is based on equations in Bruggmann et al. (2022):

$$\delta^{238}U_{auth} = \frac{\delta^{238}U_{bulk} - \delta^{238}U_{detrital}\left(\frac{U}{Al_{detrital}} \times \frac{Al}{U_{sample}}\right)}{1 - \left(\frac{U}{Al_{detrital}} \times \frac{Al}{U_{sample}}\right)} \quad (3)$$

Detrital element contributions are assumed to approximate UCC ($U/Al_{detrital} = 0.348$, McLennan, 2001; $\delta^{238}U_{detrital} = -0.29‰$, Tissot and Dauphas, 2015; Andersen et al. 2017). The resulting $\delta^{238}U_{auth}$ in the Rove and Virginia cores range from –0.52‰ to 0.53‰ (Fig. 3, Supplementary Data Table S1).

The three proximal cores record, on average, $\delta^{238}U_{auth}$ well above $\delta^{238}U_{riv}$: 89-MC-1 (0.05 ± 0.19‰, 1σ; excluding the 30 cm interval at ~86 m above the Gunflint Fm. contact; see Section 4.3), GF-3 (0.12 ± 0.12‰, 1σ), and MGS-2 (0.19 ± 0.18‰, 1σ). The deepest core (MGS-8) records $\delta^{238}U_{auth}$ of –0.13 ± 0.24‰ (1σ), which is slightly lighter than the adjacent MGS-2 core ($p = 0.04$). Core MGS-8 features only ferruginous samples, while 89-MC-1 and MGS-2 contain samples deposited under low oxygen, ferruginous and euxinic bottom waters, and GF-3 records primarily euxinic conditions (Poulton et al., 2010, 2004). Samples deposited from euxinic waters record the heaviest $\delta^{238}U_{auth}$ of 0.18 ± 0.15‰ (1σ). Samples deposited from ferruginous bottom waters have $\delta^{238}U_{auth}$ of 0.07 ± 0.18‰ (1σ), which is significantly lighter than the euxinic $\delta^{238}U_{auth}$ ($p = 0.01$), although the difference is small. Samples deposited from low-oxygen waters in the lower portion of 89-MC-1 have $\delta^{238}U_{auth}$ of –0.49 ± 0.04‰ (1σ) which is significantly lighter than the mean for ferruginous conditions ($p < 0.0001$). Table 1 and Fig. 4 summarize these findings. Additionally, $\delta^{238}U_{auth}$ tend to increase with increasing U_{EF}, Mo_{EF}, Re_{EF} and V_{EF}, and with increasing TOC (TOC data from Poulton et al., 2010) (Fig. 5).

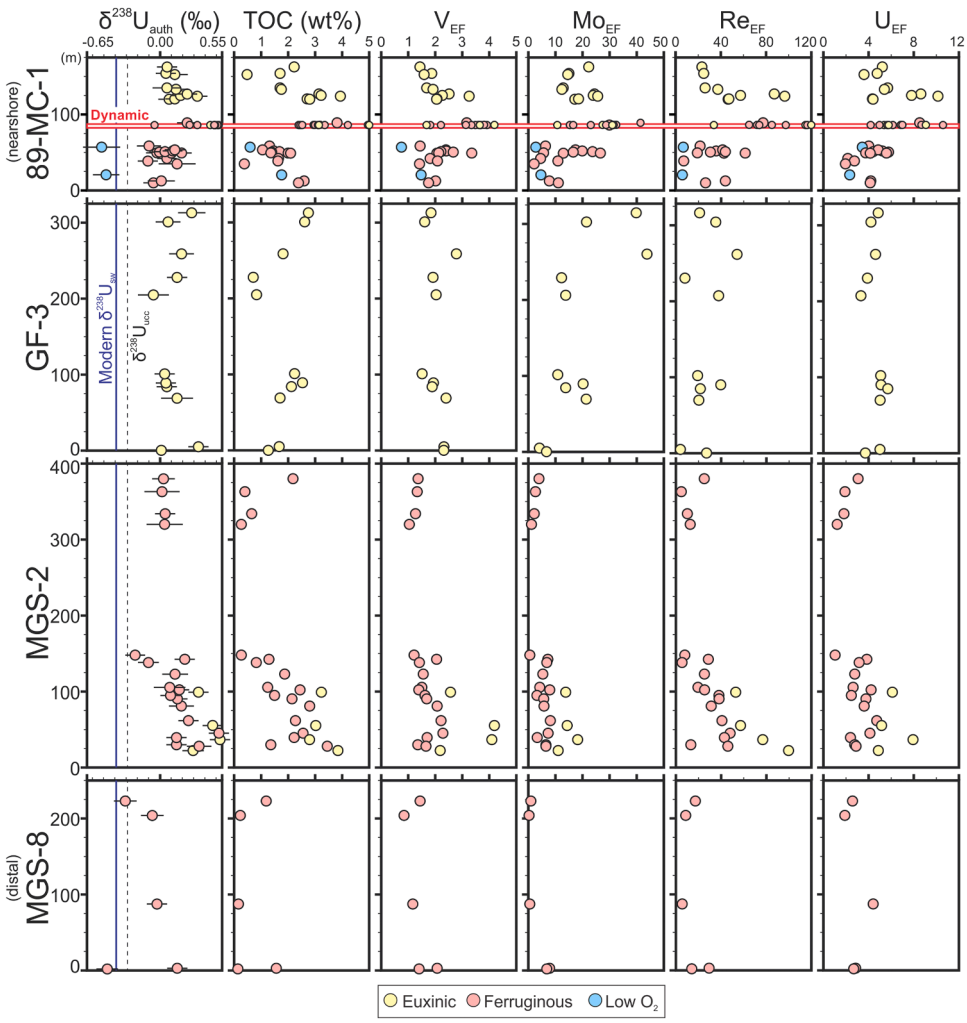

Fig. 3. Geochemical profiles for Rove/Virginia cores. Yellow markers are euxinic, red markers are ferruginous, and blue markers are low oxygen based on Fe speciation (after Poulton et al. 2004, 2010) and redox sensitive trace metal concentrations. Total organic carbon (TOC) content is from Poulton et al. (2010). Dashed vertical line in uranium isotope profiles is upper continental crust isotope composition and solid blue line is modern seawater. Error on isotope compositions is long term reproducibility of ±0.09‰ or ±2σ on replicate measurements, whichever is larger. Vertical axis is height (metres) above the contact with the Gunflint/Biwabik iron formations.

Table 1
Authigenic uranium isotope compositions ($\delta^{238}U_{auth}$) for Rove (89-MC-1, GF-3) and Virginia (MGS-2, MGS-8) formation cores in the Animikie Basin. Redox conditions are based on Fe speciation (Poulton et al. 2004, 2010). 'Dynamic' 89-MC-1 is an interval from 86.00 to 86.303 m that contains coarse pyrite grains and fluctuating redox conditions. All other samples are considered steady state with respect to redox conditions. Bracketed values are sample counts.

Core	Euxinic	Ferruginous	Low Oxygen	Mean
89-MC-1	0.14 ± 0.09‰ (10)	0.06 ± 0.11‰ (14)	–0.49 ± 0.04‰ (2)	0.05 ± 0.19‰ (26)
Dynamic	*0.44 ± 0.03‰ (2)*	*0.38 ± 0.18‰ (9)*		*0.39 ± 0.16‰ (11)*
GF-3	0.12 ± 0.12‰ (11)			
MGS-2	0.41 ± 0.11‰ (4)	0.14 ± 0.16‰ (18)		0.14 ± 0.16‰ (18)
MGS-8		–0.13 ± 0.24‰ (5)		–0.13 ± 0.24‰ (5)
All Cores	0.18 ± 0.15‰ (25)	0.07 ± 0.18‰ (37)	–0.49 ± 0.04‰ (2)	0.10 ± 0.20‰ (64)

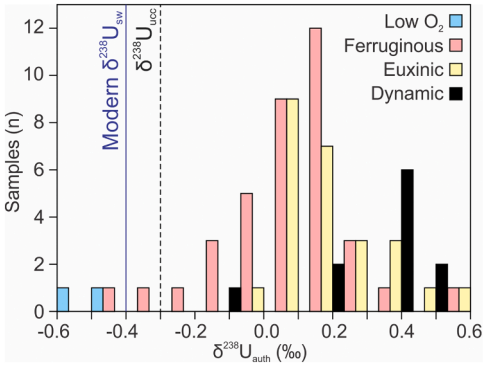

Fig. 4. Summary of authigenic U isotopic compositions by redox environments in all study cores (n = 75). 'Dynamic' refers to all samples (ferruginous and euxinic) within the dynamic interval of core 89-MC-1.

4.3. Dynamic interval in core 89-MC-1

A fluctuating redox interval of ~30 cm occurs in core 89-MC-1 (86.000–86.303 m above the Gunflint Fm. contact). This interval hosts

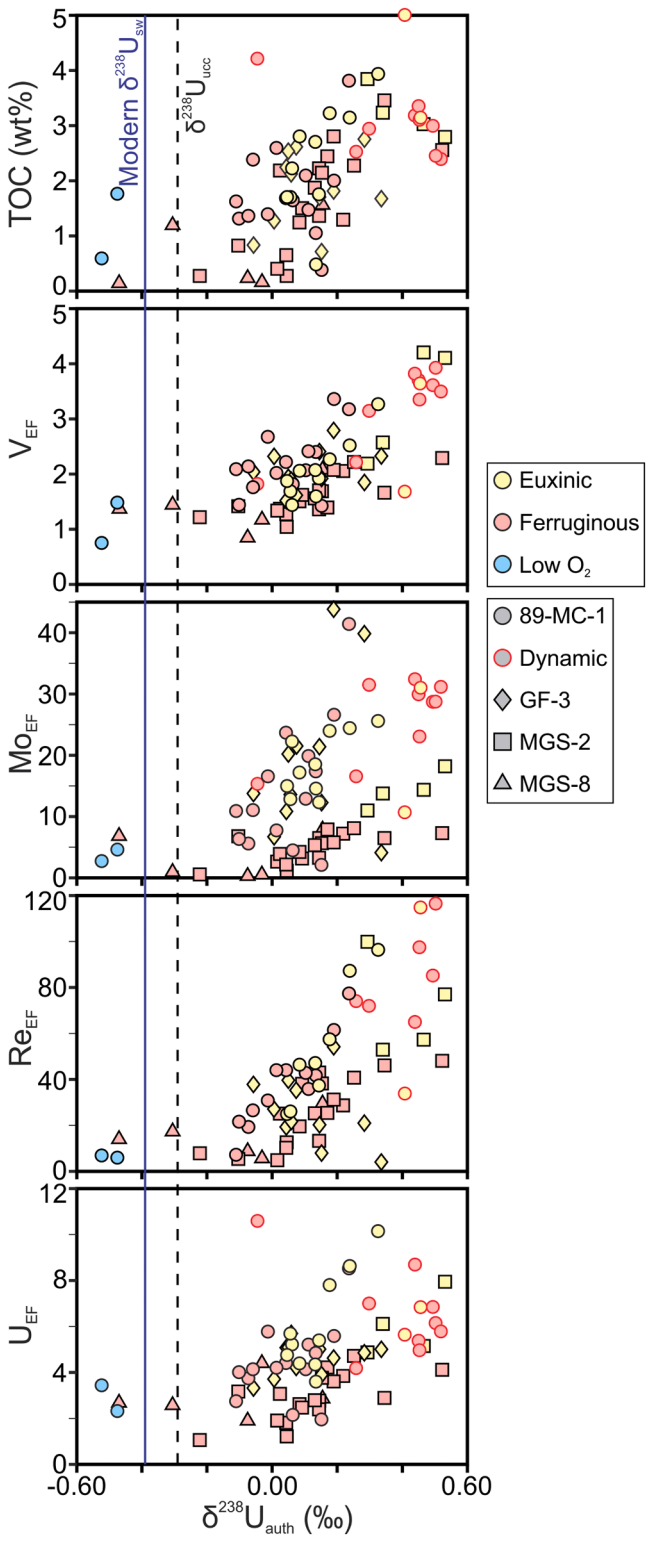

Fig. 5. Covariations between select redox sensitive trace metal enrichment factors (EF) and TOC versus $\delta^{238}U_{auth}$ for the Rove and Virginia samples. Solid blue line is modern seawater $\delta^{238}U$ and the dashed black line is modern $\delta^{238}U$ input to the oceans from rivers (derived from upper continental crust, UCC).

macroscopic pyrite clusters and layers (up to 1 mm in size; see Supplementary Fig. S1) and is interpreted to represent non-steady-state deposition under a fluctuating redoxcline during the transition to a persistently euxinic water column (Kendall et al., 2011; Poulton et al., 2004)—herein called the 'dynamic interval'. The dynamic interval features significantly ($p < 0.0001$) heavier $\delta^{238}U_{auth}$ (0.39 ± 0.16‰, 1σ) than all other samples (0.10 ± 0.20‰, 1σ) (Figs. 4 and 6). Iron speciation and RSTMs suggest that redox conditions fluctuated between ferruginous and euxinic, with most samples recording ferruginous conditions (Poulton et al., 2004). This interval is also calcareous (Ca ≤ 26 wt%) and carbonaceous (TOC ≤ 5 wt%) and includes elevated manganese (Mn ≤ 0.63 wt%), carbonate Fe (Fe_{carb} ≤ 1.4 wt%), and strontium (Sr ≤ 427 μg g^{-1}) enrichments, coincident with Ca-rich intervals (Fig. 6). Aluminium is depleted relative to UCC, especially in samples with large Ca enrichments. The Al trend is mirrored by decreased RSTM concentrations (e.g., V, Mo, Re, U) although not to values below UCC.

5. Discussion

Black shales from the Rove and Virginia formations record an extensive range of $\delta^{238}U_{auth}$, similar to observations from modern sediments (Andersen et al., 2017, 2014; Bruggmann et al., 2022; Clarkson et al., 2023; Cole et al., 2020). The heaviest $\delta^{238}U_{auth}$ recorded in these samples (0.53‰) suggests a maximum $\Delta^{238}U_{sed\text{-}sw}$ during Rove/Virginia Formation deposition of between 0.82 and 1.26‰, assuming that $\delta^{238}U_{sw}$ in the late Paleoproterozoic was not heavier than modern $\delta^{238}U_{riv}$ (–0.29‰; Andersen et al., 2017; Tissot and Dauphas, 2015) and was not lighter than the minimum $\delta^{238}U_{sw}$ estimate for the Proterozoic (–0.73‰; Gilleaudeau et al. 2019). This calculated range aligns with maximum modern isotope fractionations from anoxic, non-diffusion-limited, and/or temporally dynamic marine redox settings (Andersen et al., 2017, 2014; Clarkson et al., 2023; Rutledge et al., 2024). It has been suggested that non-uniformitarian U isotope systematics, such as smaller fractionation factors, alternative mechanisms and/or efficiency of U incorporation into black shales, occurred in the Proterozoic ocean (Chen et al., 2021). However, our data show that large U isotope fractionations associated with reduction and removal of U into organic-sediments, akin to those observed for modern and Phanerozoic organic-rich sediments, were prevalent in the late Paleoproterozoic ocean. Below, we discuss possible mechanisms for highly variable isotopic fractionations in the Late Paleoproterozoic under primarily anoxic conditions.

5.1. Effects of local microbial activity, aqueous chemistry, and sedimentary processes on uranium isotope fractionation in the late paleoproterozoic ocean

In cores recording changing redox conditions (89-MC-1, MGS-2), $\delta^{238}U_{auth}$ tend to scale with local redox conditions inferred from Fe speciation and RSTM contents, such that euxinic settings generally have heavier $\delta^{238}U_{auth}$ compared to non-euxinic settings (Fig. 3). Considering all cores, euxinic and ferruginous $\delta^{238}U_{auth}$ data overlap (Fig. 4), suggesting that other controls beyond the redox environment impacted $\delta^{238}U_{auth}$. We hypothesize that several local controls on U isotopic fractionation were operating in the Animikie Basin, which we consider below.

5.1.1. Microbial role in large uranium isotope fractionations

Some modern microbes (e.g., *Shewanella oneidensis* MR-1, *Desulfovibrio desulfuricans*) have been observed using U(VI) as electron acceptors in their metabolism (Liu et al., 2002; Marshall et al., 2006). These dissimilatory metal reducing bacteria dominate under anaerobic conditions (most are also iron, FeRB, or sulfate, SRB, reducers), although some can grow aerobically (e.g., *Shewanella algae*, Dang et al., 2016). Biotic reduction can induce an isotopic fractionation, $\Delta^{238}U_{(IV)\text{–}(VI)}$, of 0.7–1.0‰ as $U(VI)_{aq}$ is reduced to solid U(IV) phases (Basu et al., 2014; Stylo et al., 2015). The Animikie Basin euxinic wedge likely developed due to abundant organic matter delivery to the sediment–water interface, as evidenced by TOC of 2.3 ± 0.9 wt% (1σ) in euxinic samples above 100 m in 89-MC-1, throughout GF-3 and periodically in the lower

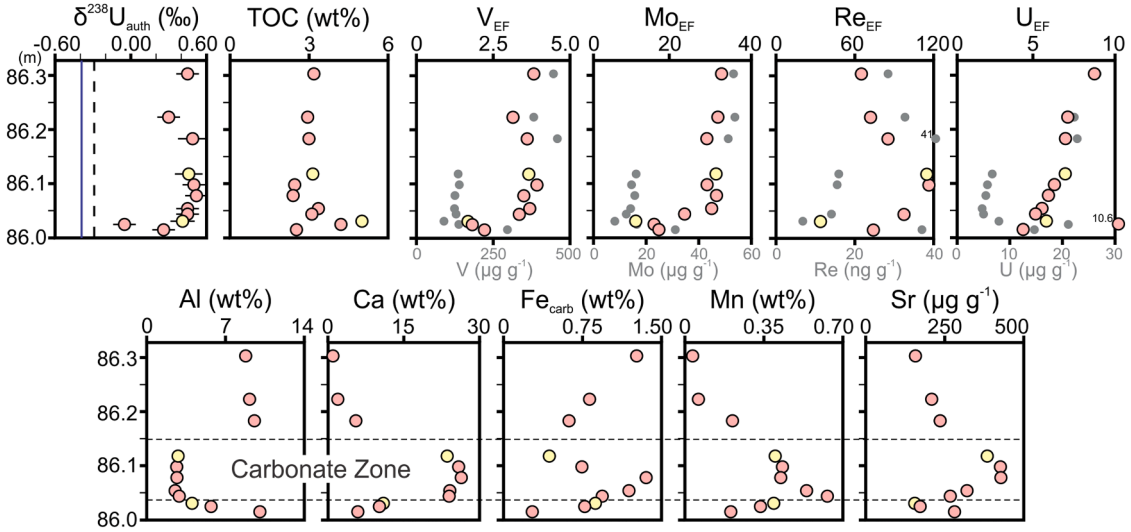

Fig. 6. Uranium isotope and elemental profiles for the dynamic interval within 89-MC-1. Marker colour represents local redox conditions based on Fe speciation from Poulton et al. 2010, as described in previous figures. Grey markers are elemental concentrations (V, Mo, Re and U). Solid blue line in $\delta^{238}U_{auth}$ profile is modern seawater composition, and dashed line is upper continental crust. Vertical axis is height above the top of the Gunflint iron formation in metres.

125 m of MGS-2. Additionally, pyrite sulfur isotopes ($\delta^{34}S_{py}$) in these samples approach Paleoproterozoic $\delta^{34}S_{sw}$ of ~17‰, suggesting very low seawater sulfate concentrations (Poulton et al., 2010). Thus, the conditions were appropriate for microbial sulfate (and uranium) reduction within the euxinic wedge. Mean $\delta^{238}U_{auth}$ in these samples is 0.18 ± 0.15‰ (1σ). Thus, $\Delta^{238}U_{eux\text{-}sw}$ in the Animikie Basin may have been on average 0.47–0.91‰, if $\delta^{238}U_{sw}$ was either unfractionated from modern $\delta^{238}U_{riv}$ or was similar to the minimum $\delta^{238}U_{sw}$ estimate from Proterozoic carbonates. This range of isotopic fractionations overlaps with those observed in bio-reduction experiments (Basu et al., 2014; Stylo et al., 2015).

Ferruginous intervals stratigraphically or laterally adjacent to the euxinic wedge also record $\delta^{238}U_{auth}$ heavier than $\delta^{238}U_{riv}$, suggesting continued U isotope fractionation. Because euxinia would have occurred due to SRB activity, we infer that U isotopic fractionation just outside the euxinic wedge was also driven, at least in part, by microbial activity. There is currently no evidence that isotopic fractionations during microbial U(VI) reduction differ between Fe(III) and SO_4^{2-}-rich conditions, with one field-scale experiment demonstrating Rayleigh fractionation with isotopic enrichment of 0.65‰ under both conditions (Shiel et al., 2016). Additionally, ferruginous Paleozoic shales have recorded highly variable $\delta^{238}U_{auth}$ (–0.05 ± 0.46‰, up to 0.57‰) positively correlated with TOC, that suggests locally-driven isotope fractionations of, on average, ~0.4‰ and up to ~1.0‰, based on coeval $\delta^{238}U_{carb}$ (Cole et al., 2020; Rutledge et al., 2024). In the Rove and Virginia formations, ferruginous samples with elevated TOC (1.9 ± 0.8 wt%, 1σ; denoted as 'ferrTOC') are found below 100 m in 89-MC-1 and 125 m in MGS-2. Mean $\delta^{238}U_{auth}$ in these intervals is 0.13 ± 0.14‰ (1σ); thus, $\Delta^{238}U_{ferrTOC\text{–}sw}$ may have reached 0.42–0.86‰, assuming $\delta^{238}U_{sw}$ was between modern $\delta^{238}U_{riv}$ (–0.29‰) and the minimum estimated Proterozoic $\delta^{238}U_{sw}$ (–0.73‰). Neither $\Delta^{238}U$ nor TOC are significantly different between the euxinic wedge and adjacent high TOC ferruginous environments ($p = 0.18$ for both parameters).

Low-oxygen samples in 89-MC-1, and deep-water ferruginous samples in MGS-8 and above 125 m in MGS-2, have significantly lower TOC (0.8 ± 0.7 wt%, 1σ; $p < 0.001$) and RSTM contents than the euxinic wedge and adjacent environments (denoted as 'lowerTOC'), and $\delta^{238}U_{auth}$ is significantly lower (–0.10 ± 0.25‰, 1σ; $p < 0.001$). In these cases, $\Delta^{238}U_{lowerTOC\text{–}sw}$ may have been 0.19–0.63‰, based on a seawater range from modern $\delta^{238}U_{riv}$ to the minimum estimated Proterozoic $\delta^{238}U_{sw}$ value. Although the maximum estimated offset is within the range of bio-reduction, the smaller $\Delta^{238}U_{lowerTOC\text{–}sw}$ for the majority of these samples suggests that microbially mediated reduction was not the dominant mechanism for U enrichment or isotope fractionation, at least not to the extent inferred for the euxinic wedge and adjacent areas. When electron donors (e.g., lactate, acetate) are limited but microbial reduction still occurs, U isotopic fractionations will be large as the electron flux and ultimately reduction rate decreases (Basu et al., 2020). However, if electron donor availability was very low, as expected for lower TOC samples, then microbial activity may have been limited. This could explain the lighter $\delta^{238}U_{auth}$ for such samples, especially if U(VI) reduction occurred via alternative abiotic processes as explored below.

5.1.2. *Abiotic uranium reduction as a driver of uranium isotope fractionations*

Recent experimental studies have demonstrated U isotopic fractionations by abiotic reduction, although the magnitude of isotopic fractionation varies by reductant and aqueous U speciation (Brown et al., 2018; Stylo et al., 2015; Wang et al., 2015). Some experiments have revealed only small or opposing (^{238}U preferentially in the $U(VI)_{aq}$ phase) isotope fractionations during abiotic reduction by Fe(II) phases (e.g., mackinawite, magnetite) and aqueous Fe^{2+} or HS^-, potentially associated with non-NVE kinetic isotopic effects (Stylo et al., 2015). Others have shown that abiotic U isotope fractionation is affected by aqueous U speciation, primarily where increased $[Ca^{2+}]_{aq}$ results in preferential formation of aqueous $Ca_2UO_2(CO_3)_3^0$, which does not readily adsorb to solid reductant surfaces compared to anionic species such as $UO_2(CO_3)_2^{2-}$ (Brown et al., 2018). This slows reaction kinetics and promotes equilibrium exchange between $U(VI)_{aq}$ and reduced U $(IV)_s$ phases, causing larger isotopic fractionations comparable to those observed in biotic experiments (cf. Brown et al., 2018; Stylo et al., 2015). Conversely, U_{aq} as $Ca_2UO_2(CO_3)_3^0$ can inhibit U(VI) reduction by Fe_{aq}^{2+} (Dewey et al., 2020), an inferred effect in a modern low-productivity ferruginous lake, where both oxic and ferruginous sediment $\delta^{238}U$ was near upper continental crust composition, and ~40% of the bottom water U_{aq} was present as $CaUO_2(CO_3)_3^0$ (Gilleaudeau et al., 2025). Large empirical isotope fractionations (up to 1.6‰) have also been observed during equilibrium isotopic exchange between $U(VI)_{aq}$–$U(IV)_{aq}$ and $U(VI)_{aq}$–$U(IV)_s$ (Wang et al., 2015). Thus, abiotic reductive isotope fractionation can be defined by a balance between kinetic and equilibrium endmembers, where a kinetic-dominated system (e.g., rapid reduction with minimal isotopic exchange between U (VI) and U(IV) phases) results in limited isotope fractionation, and an

equilibrium-dominated system (e.g., slower reduction with abundant U (VI)–U(IV) isotopic exchange) results in larger isotope fractionations (Brown et al., 2018).

Abiotic U(VI) reduction into Animikie Basin sediments is a plausible pathway to enrich U and induce U isotopic fractionation, given an inferred abundance of potential reductants such as aqueous Fe^{2+}, or solid phase ferrous and/or sulfide minerals. If such conditions were maintained, it is expected that abiotic reduction rates would be rapid and resulting U isotope fractionations would be small, unless Ca^{2+} was also widely available (> 1 mM; Brown et al., 2018) to form neutrally charged Ca-uranyl carbonates. Chen et al. (2021) modeled temporal variations in neutral versus anionic uranyl carbonates and found that, at ~1800 Ma, $Ca_2UO_2(CO_3)_3^0$ may have comprised >60% of aqueous uranyl carbonates versus modern seawater at ~44%. Experiments of U reduction by synthetic mackinawite (FeS) depict a relationship between the proportion of Ca-uranyl carbonate and resulting abiotic isotope fractionation ($\Delta^{238}U = 0.854 \times \%U_{neutral} + 0.2$; Brown et al. 2018), thus isotopic fractionations of >0.7‰ during abiotic reduction by mackinawite may have been possible at ~1800 Ma. In high-productivity environments, isotopically heavy U(IV) may be further associated with sinking organic matter, which was thought to be a primary control on $\delta^{238}U_{auth}$ in some Paleozoic black shales based on strong positive $\delta^{238}U_{auth}$–TOC relationships (Rutledge et al., 2024).

In deeper water ferruginous locations (MGS-8, above 125 m in MGS-2), U isotope fractionation appears to have been small given light $\delta^{238}U_{auth}$, but moderate U_{EF} values suggest enrichment of U in the sediment. Microbial reduction may have been less important in these locations, given that generally lower TOC (0.8 ± 0.7 wt%, 1σ) compared to within and near the euxinic wedge suggests less organic reductants for anaerobic respiration. Instead, rapid abiotic U(VI) reduction may have occurred via reaction with aqueous Fe^{2+} upwelled from deeper hydrothermal sources causing limited (or negative) U isotope fractionation from seawater (Brown et al., 2018; Du et al., 2011; Stylo et al., 2015). Alternatively, or additionally, U(VI) adsorption to solid organic matter or Fe/Mn species resulting in negative or no isotopic fractionation (Brennecka et al., 2011; Chen et al., 2020; Dang et al., 2016; Gilleaudeau et al., 2025) could be responsible for light $\delta^{238}U_{auth}$ and moderate U_{EF}. This would be particularly relevant in an environment where Fe^{2+} was the primary reductant and $[Ca^{2+}_{aq}]$ was elevated, as the presence of Ca-uranyl-carbonates can inhibit U(VI) reduction by Fe^{2+} (Dewey et al., 2020).

5.1.3. Controls on very high $\delta^{238}U_{auth}$ in animikie basin sediments

The dynamic interval in 89-MC-1 exhibits very heavy $\delta^{238}U_{auth}$, averaging 0.39 ± 0.16‰ (1σ), corresponding to a potential $\Delta^{238}U_{dynamic\text{-}sw}$ of 0.68–1.12‰ if $\delta^{238}U_{sw}$ were between the modern $\delta^{238}U_{riv}$ (–0.29‰) and minimum estimated mid-Proterozoic $\delta^{238}U_{sw}$ (–0.73‰) values. Clarkson et al. (2023) observed similarly elevated $\Delta^{238}U_{sed\text{-}sw}$ near the intrinsic fractionation factor across the Black Sea chemocline, with low to moderate TOC accumulation, low U accumulation, and lower H_2S concentrations. The Black Sea chemocline samples also feature $\delta^{98}Mo$ lighter than modern seawater, corresponding to weaker euxinia or H_2S limited to porewaters at this location. These conditions were hypothesised to contribute to high $\Delta^{238}U_{sed\text{-}sw}$ by several possible mechanisms, including removal of a diffusive isotopic fractionation effect if U reduction occurred at the sediment–water interface (e.g., within a permeable organic floc layer) or rapid sedimentation isolating an interval from U isotopic diffusion from bottom water to porewater.

Like the Black Sea samples, the dynamic interval in 89-MC-1 features low to moderate TOC, low [U] (note that U_{EF} does not demonstrate depletion due to a corresponding decrease in local [Al]), and $\delta^{98}Mo$ is notably lighter than the maximum reported values in fully euxinic sediments of the upper portion of 89-MC-1 (Kendall et al., 2011). Additionally, this interval hosts macroscopic pyrite, and Fe speciation indicates variable local redox conditions, suggesting Fe^{2+}–H_2S chemocline fluctuations near the sediment–water interface (Kendall et al., 2011; Poulton et al., 2010). As the TOC content at the base of this interval is also elevated (up to 5.0 wt%), a sizable organic carbon deposition event may have occurred, possibly resulting in U reduction in a highly permeable organic floc allowing for a larger expression of the reductive isotopic fractionation effect. Simultaneously, organic matter deposition would provide substrate for SRB and thus microbial-derived H_2S, Fe(II) and HCO_3^-. These circumstances would have allowed for the formation of pyrite and carbonate phases such as calcite or aragonite ($CaCO_3$), siderite ($Fe^{(2+)}CO_3$), rhodochrosite ($Mn^{(2+)}CO_3$), and strontianite ($SrCO_3$), imparting the corresponding observed elevated elemental concentrations (Fig. 6). This could have exacerbated the formation of Ca-uranyl-carbonates that would slow reduction rates and further increase the $\Delta^{238}U_{sed\text{-}sw}$ by equilibrium isotopic exchange between $U(IV)_s$ and $U(VI)_{aq}$.

5.1.4. Heterogeneity of late paleoproterozoic U_{sw} supply and reservoir

Precambrian shales feature very low U_{auth} (mean < 1 μg g^{-1}; excluding shales deposited during the Great Oxidation and Lomagundi events) compared to Phanerozoic shales (mean ~25 μg g^{-1}), attributed to low atmospheric O_2 limiting oxidation of immobile continental U(IV), thus hindering mobile U(VI) supply to the oceans (Partin et al., 2013). A lack of supply, coupled with a widely anoxic or highly productive ocean with enhanced U burial could have resulted in U_{sw} residence times near the average ocean mixing time and thus heterogeneous $[U]_{sw}$ and $\delta^{238}U_{sw}$ (Chen et al., 2021). As rivers are the main source of U to the oceans, $[U]_{sw}$ would generally decline moving offshore. Regional variations in $\delta^{238}U_{riv}$ (as observed in river systems today; Andersen et al., 2016) and marine isotope fractionation associated with U burial in sediments (amplified by high primary productivity) would cause heterogeneous $\delta^{238}U_{sw}$. The nearshore–offshore transition would be marked by a decrease in continentally-supplied nutrients and thus waning productivity and TOC flux with distance from the shoreline, which has been incorporated algorithmically or pseudo-spatially into previous elemental mass balances for Mo, Cr and Re (Reinhard et al., 2013; Sheen et al., 2018). Together, these spatial factors may have influenced the observed trends in U_{EF}, TOC and $\delta^{238}U_{auth}$ across the Animikie Basin transect. The proximal cores 89-MC-1 (excluding the dynamic interval) and GF-3 feature a combined U_{EF} of 4.8 ± 1.7, while distal cores MGS-2 and MGS-8 feature a lower combined U_{EF} of 3.4 ± 1.5. The TOC content also decreases with distance from the shoreline, although a significant decrease only occurs in the most distal core MGS-8 (0.6 ± 0.7 wt%, versus 1.9 ± 0.9 wt% in the three proximal locations). This trend does not hold for $\delta^{238}U_{auth}$ in the three proximal cores, where MGS-2 features, on average, heavier $\delta^{238}U_{auth}$ than 89-MC-1 and GF-3, however, distal core MGS-8 does host the lightest $\delta^{238}U_{auth}$ samples. Thus, it is likely that beyond local isotope fractionation resulting in variable and/or heavy $\delta^{238}U_{auth}$ (see sections 5.1.1–5.1.3), U and TOC supply affected $\delta^{238}U_{auth}$, primarily towards the deepest portion of the basin. A smaller TOC supply would limit microbial activity and accompanying large isotopic fractionation or shift the balance of U reduction to a diffusion-limited regime in sediments rather than a non-diffusion-limited regime in a permeable organic floc as suggested by Clarkson et al. (2023). If U_{sw} was depleted towards MGS-8, quantitative U removal into sediments is expected, provided availability of reducing agents such as upwelling Fe(II), negating isotopic fractionation effects and resulting in $\delta^{238}U_{auth}$ approaching $\delta^{238}U_{sw}$.

5.2. Unified animikie basin uranium isotope model

Based on observed U_{EF} and $\delta^{238}U_{auth}$, and suggested mechanisms for U enrichments and isotopic fractionations, we propose that U isotope systematics in the late Paleoproterozoic ocean were primarily governed by the relative importance of microbially mediated reduction versus abiotic reduction and/or adsorption. This interpretation is supported by positive relationships between $\delta^{238}U_{auth}$–TOC (Fig. 5), and significantly elevated $\delta^{238}U_{auth}$, TOC, and U_{EF} in euxinic wedge/adjacent higher-TOC

ferruginous samples compared to shallow water low-oxygen and deeper water lower-TOC ferruginous samples ($p < 0.001$). Productivity has previously been suggested to exert a primary control on $\delta^{238}U_{auth}$ in Paleozoic black shales, identified by strong correlation between $\delta^{238}U_{auth}$ and TOC, and productivity proxies such as Zn and Ni (Rutledge et al., 2024). In the shallower shelf locations where abundant organic matter was deposited and a euxinic wedge developed, we anticipate vigorous microbial reduction of U(VI) coupled with FeRB and SRB activity, resulting in elevated U enrichment and large isotopic fractionations, similar to those observed in microbial batch experiments and modern euxinic environments ($\Delta^{238}U_{solid\text{-}aqueous}$ from 0.4‰ to 1.0‰; Andersen et al., 2017; Basu et al., 2020, 2014; Holmden et al., 2015; Rolison et al., 2017; Stylo et al., 2015). These locations may also experience non-diffusion-limited conditions where U reduction occurs near the sediment–water interface, likely within a permeable organic floc (Clarkson et al., 2023).

Abiotic reduction or U(VI) adsorption to solid organic matter or Fe/Mn species likely dominated in shallower low-oxygen and deeper lower-TOC ferruginous environments. Isotopic fractionation is anticipated to have been limited, even when U enrichment was elevated, because of rapid reduction rates when abundant abiotic reductants were available, or due to increased U adsorption to solid Fe/Mn species which imparts little or no isotopic fractionation (Gilleaudeau et al., 2025). We do not discount the potential for multiple reduction pathways, including simultaneous biotic and abiotic processes. Rather, we suggest that observed $\delta^{238}U_{auth}$ throughout the Animikie Basin resulted from a balance between these processes. Microbial activity may be primarily responsible for large isotope fractionations, but these may be compounded by slow abiotic reduction, perhaps in the presence of substantial Ca^{2+}. Additionally, we suggest that temporary non-diffusion-limited conditions could have contributed to unusually high $\delta^{238}U_{auth}$ in the dynamic interval. Fig. 7 provides a summary of proposed mechanisms and the locations where each mechanism may have dominated.

5.3. Significance for the global uranium isotope mass balance of the Proterozoic ocean

Beyond the Animikie Basin, these findings can help reconcile potentially modern-like Proterozoic $\delta^{238}U_{sw}$ within the extensive anoxic conditions of the Proterozoic oceans (Chen et al., 2021; Gilleaudeau et al., 2019). By the conventional global U isotope mass balance, a widely anoxic ocean should result in very light $\delta^{238}U_{sw}$ due to the preferential burial of ^{238}U in anoxic sediments. Instead, we observe that heavy $\delta^{238}U_{auth}$ in the late Paleoproterozoic ocean primarily occurred in settings where organic matter was abundant closer to the paleoshoreline. In Paleoproterozoic deeper shelf areas, where lower productivity and ferruginous conditions prevailed, limited U isotope fractionation is expected based on the Animikie Basin data and supported by modern lacustrine data (Gilleaudeau et al., 2025). Hence, a widely anoxic ocean does not necessarily have very light $\delta^{238}U_{sw}$, as alluded to by Chen et al. (2021). Light Proterozoic $\delta^{238}U_{sw}$ may be achieved when primary productivity rates are elevated and could induce vigorous U reduction and isotopic fractionation under high-TOC ferruginous or euxinic conditions, in contrast to times with suppressed primary productivity when Proterozoic $\delta^{238}U_{sw}$ may have been more modern-like. Seafloor reconstructions from the U isotope mass balance may therefore reflect areas where localized conditions (e.g., productivity-driven anoxia) affect U reduction, rather than discrete redox conditions such as ferruginous anoxia or euxinia, although the precise redox conditions may still impact isotopic fractionations in settings where environmental conditions were otherwise generally stable.

The large variability in $\delta^{238}U_{auth}$ in the Rove/Virginia formations and other Proterozoic black shales inhibits their use as direct records of Proterozoic $\delta^{238}U_{sw}$. However, as demonstrated here, they are useful for inferring whether large isotopic fractionations occurred in ancient environments. During Rove/Virginia deposition, $\delta^{238}U_{sw}$ may have been relatively light based on contemporaneous $\delta^{238}U_{carb}$ from the Australian Duck Creek Formation, which was close to the minimum Proterozoic estimate. With such light $\delta^{238}U_{sw}$ and large observed local U isotopic fractionations in the Animikie Basin, it is plausible that the late Paleoproterozoic ocean at ~1840 Ma experienced enhanced primary productivity and development of euxinic wedges on continental margins, potentially covering up to 10% of the global seafloor (see mass balance in the Supplementary Material). This hypothesis is supported by elevated organic C/P ratios in euxinic Animikie Basin sediments, suggesting enhanced P-cycling at this time (Guilbaud et al., 2020). At other times, the Proterozoic oceans are thought to have been largely P-limited due to reduced P input flux and potential co-precipitation with or adsorption to Fe-minerals (Laakso and Schrag, 2014). These low-productivity oceans would be reflected in the Proterozoic when $\delta^{238}U_{carb}$ and $\delta^{238}U_{auth}$ are not appreciably different from modern average $\delta^{238}U_{sw}$ and $\delta^{238}U_{riv}$.

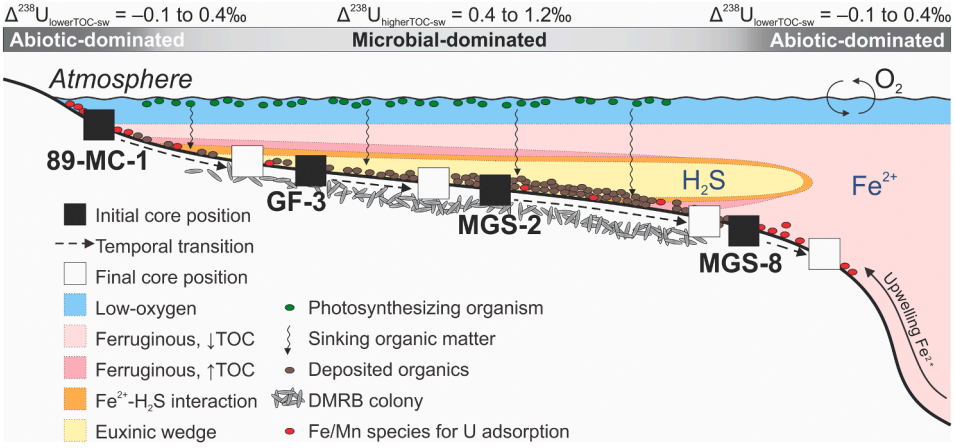

Fig. 7. Model of the Animikie Basin summarizing the controls on sedimentary uranium isotope offsets from seawater ($\Delta_{sed\text{-}sw}$). These offsets are based on $\delta^{238}U_{auth}$ observed in Animikie Basin cores and their corresponding $\Delta^{238}U_{sed\text{-}sw}$ range using minimum Proterozoic $\delta^{238}U_{sw}$ and modern $\delta^{238}U_{riv}$. Black squares are the approximate initial positions of the four drill cores and white squares are their approximate final positions. Note that these represent temporal, rather than spatial transitions as sea level transgressed and bottom water conditions at each location migrated landward. Diagram not to scale. DMRB = dissimilatory metal reducing bacteria.

6. Conclusions

Study of the Animikie Basin has progressed our understanding of late Paleoproterozoic ocean conditions, with its well-preserved sedimentary succession and growing geochemical database. Black shale $\delta^{238}U_{auth}$ varies with redox conditions within each of the four studied drill cores but are inconsistent between redox settings across the basin. We attribute the basin-scale $\delta^{238}U_{auth}$ variations to local controls, primarily related to organic matter flux to the sediment–water interface. Where organic matter accumulation was large, U reduction by dissimilatory metal reducing bacteria during organic carbon degradation could have resulted in large U isotope fractionations and heavy sedimentary $\delta^{238}U$. Where organic matter accumulation was lower, U reduction would have been minimal or occurred rapidly by abiotic reductants like Fe^{2+}_{aq}, producing small effective U isotope fractionations. Limited U reduction is hypothesised in shallower locations where O_2 could be maintained at low concentrations or perhaps in deeper settings where U was instead enriched in sediments by adsorption to organic matter or Fe/Mn species without appreciable isotopic fractionation.

These findings help improve our understanding of the global U isotope mass balance, whose application to Proterozoic ocean reconstructions has been questioned due to apparent contradictions between carbonate and black shale isotopic records. We have demonstrated that $\delta^{238}U_{sw}$ could have maintained near-modern compositions in a Proterozoic ocean that was predominantly anoxic but lacked organic carbon fluxes to sediments (from elevated primary productivity), diminishing the development of highly reducing environments suitable for U reduction and isotopic fractionation, and thus keeping $\delta^{238}U_{sw}$ close to $\delta^{238}U_{riv}$. Conversely, episodes of enhanced primary productivity could promote conditions for vigorous U reduction in the Proterozoic oceans, increasing preferential burial of ^{238}U in sediments, thus driving $\delta^{238}U_{sw}$ to lower values. Hence, more generally, the U isotope system in Proterozoic black shales can be employed as a proxy for anoxia in highly productive continental margins.

CRediT authorship contribution statement

Alexandra Kunert: Writing – review & editing, Writing – original draft, Visualization, Validation, Software, Resources, Project administration, Methodology, Investigation, Formal analysis, Data curation, Conceptualization. **Simon W. Poulton:** Writing – review & editing, Resources. **Donald E. Canfield:** Writing – review & editing, Resources. **Philip W. Fralick:** Writing – review & editing, Resources. **Geoffrey J. Gilleaudeau:** Writing – review & editing, Supervision. **Brian Kendall:** Writing – review & editing, Supervision, Resources, Project administration, Methodology, Funding acquisition, Conceptualization.

Declaration of competing interest

The authors declare that they have no known competing financial interests or personal relationships that could have appeared to influence the work reported in this paper.

Acknowledgments

The authors thank the editor for manuscript handling, as well as Michael Kipp and one anonymous reviewer for providing critical feedback that improved the manuscript. AK was supported by a Natural Science and Engineering Research Council of Canada (NSERC) Canada Graduate/Post-Graduate Scholarship–Doctoral. BK acknowledges support from the Canada Research Chairs program (CRC-2018-00039) and a NSERC Discovery Grant (RGPIN-2019-0409). SWP was supported in part by the World Research Hub (WRH) Program of the International Research Frontiers Initiative, Tokyo Institute of Technology. DEC acknowledges support from the Villum Foundation (grant 54433). PF was funded by a NSERC Discovery Grant. GJG is grateful for financial support from the NASA Exobiology Program, the NSF Geobiology and Low-Temperature Geochemistry Program, and the American Chemical Society Petroleum Research Fund.

Supplementary materials

Supplementary material associated with this article can be found, in the online version, at doi:10.1016/j.epsl.2025.119498.

Data availability

Data is available in the attached supplementary spreadsheet.

References

Addison, W.D., Brumpton, G.R., Vallini, D.A., McNaughton, N.J., Davis, D.W., Kissin, S. A., Fralick, P.W., Hammond, A.L., 2005. Discovery of distal ejecta from the 1850 Ma Sudbury impact event. Geology. 33, 193–196. https://doi.org/10.1130/G21048.1.

Andersen, M.B., Romaniello, S., Vance, D., Little, S.H., Herdman, R., Lyons, T.W., 2014. A modern framework for the interpretation of 238U/235U in studies of ancient ocean redox. Earth. Planet. Sci. Lett. 400, 184–194. https://doi.org/10.1016/J.EPSL.2014.05.051.

Andersen, M.B., Stirling, C.H., Weyer, S., 2017. Uranium isotope fractionation. Rev. Mineral. Geochem. 82, 799–850. https://doi.org/10.2138/rmg.2017.82.19.

Andersen, M.B., Vance, D., Morford, J.L., Bura-Nakić, E., Breitenbach, S.F.M., Och, L., 2016. Closing in on the marine 238U/235U budget. Chem. Geol. 420, 11–22.

Asael, D., Tissot, F.L.H., Reinhard, C.T., Rouxel, O., Dauphas, N., Lyons, T.W., Ponzevera, E., Liorzou, C., Chéron, S., 2013. Coupled molybdenum, iron and uranium stable isotopes as oceanic paleoredox proxies during the Paleoproterozoic Shunga Event. Chem. Geol. 362, 193–210. https://doi.org/10.1016/J.CHEMGEO.2013.08.003.

Basu, A., Sanford, R.A., Johnson, T.M., Lundstrom, C.C., Löffler, F.E., 2014. Uranium isotopic fractionation factors during U(VI) reduction by bacterial isolates. Geochim. Cosmochim. Acta 136, 100–113. https://doi.org/10.1016/J.GCA.2014.02.041.

Basu, A., Wanner, C., Johnson, T.M., Lundstrom, C.C., Sanford, R.A., Sonnenthal, E.L., Boyanov, M.I., Kemner, K.M., 2020. Microbial U isotope fractionation depends on the U(VI) reduction rate. Environ. Sci. Technol. 54, 2295–2303. https://doi.org/10.1021/ACS.EST.9B05935.

Brennecka, G.A., Wasylenki, L.E., Bargar, J.R., Weyer, S., Anbar, A.D., 2011. Uranium isotope fractionation during adsorption to Mn-oxyhydroxides. Environ. Sci. Technol. 45, 1370–1375. https://doi.org/10.1021/es103061v.

Brown, S.T., Basu, A., Ding, X., Christensen, J.N., DePaolo, D.J., 2018. Uranium isotope fractionation by abiotic reductive precipitation. Proc. Natl. Acad. Sci. u S. a 115, 8688–8693. https://doi.org/10.1073/PNAS.1805234115.

Bruggmann, S., Gilleaudeau, G.J., Romaniello, S.J., Severmann, S., Canfield, D.E., Anbar, A.D., Scholz, F., Frei, R., 2022. Uranium isotope cycling on the highly productive Peruvian margin. Chem. Geol. 590, 120705. https://doi.org/10.1016/j.chemgeo.2021.120705.

Brüske, A., Weyer, S., Zhao, M.Y., Planavsky, N.J., Wegwerth, A., Neubert, N., Dellwig, O., Lau, K.V., Lyons, T.W., 2020. Correlated molybdenum and uranium isotope signatures in modern anoxic sediments: implications for their use as Paleoredox proxy. Geochim. Cosmochim. Acta 270, 449–474. https://doi.org/10.1016/J.GCA.2019.11.031.

Chen, X., Romaniello, S.J., Herrmann, A.D., Hardisty, D., Gill, B.C., Anbar, A.D., 2018. Diagenetic effects on uranium isotope fractionation in carbonate sediments from the Bahamas. Geochim. Cosmochim. Acta 237, 294–311. https://doi.org/10.1016/J.GCA.2018.06.026.

Chen, X., Romaniello, S.J., Herrmann, A.D., Wasylenki, L.E., Anbar, A.D., 2016. Uranium isotope fractionation during coprecipitation with aragonite and calcite. Geochim. Cosmochim. Acta 188, 189–207. https://doi.org/10.1016/j.gca.2016.05.022.

Chen, X., Tissot, F.L.H., Jansen, M.F., Bekker, A., Liu, C.X., Nie, N.X., Halverson, G.P., Veizer, J., Dauphas, N., 2021. The uranium isotopic record of shales and carbonates through geologic time. Geochim. Cosmochim. Acta 300, 164–191. https://doi.org/10.1016/j.gca.2021.01.040.

Chen, X., Zheng, W., Anbar, A.D., 2020. Uranium isotope fractionation (238U/235U) during U(VI) uptake by freshwater Plankton. Environ. Sci. Technol. 54, 2744–2752. https://doi.org/10.1021/ACS.EST.9B06421/ASSET/IMAGES/MEDIUM/ES9B06421_M006.GIF.

Cheng, K., Elrick, M., Romaniello, S.J., 2020. Early Mississippian ocean anoxia triggered organic carbon burial and late Paleozoic cooling: Evidence from uranium isotopes recorded in marine limestone. Geology. 48, 363–367. https://doi.org/10.1130/G46950.1.

Clarkson, M.O., Sweere, T.C., Chiu, C.F., Hennekam, R., Bowyer, F., Wood, R.A., 2023. Environmental controls on very high δ238U values in reducing sediments: Implications for Neoproterozoic seawater records. Earth. Sci. Rev. 237, 104306. https://doi.org/10.1016/J.EARSCIREV.2022.104306.

Cole, D.B., Planavsky, N.J., Longley, M., Böning, P., Wilkes, D., Wang, X., Swanner, E.D., Wittkop, C., Loydell, D.K., Busigny, V., Knudsen, A.C., Sperling, E.A., 2020. Uranium isotope fractionation in non-sulfidic anoxic settings and the global uranium isotope mass balance. Glob. Biogeochem. Cycles. 34, e2020GB006649. https://doi.org/10.1029/2020GB006649.

Dahl, T.W., Boyle, R.A., Canfield, D.E., Connelly, J.N., Gill, B.C., Lenton, T.M., Bizzarro, M., 2014. Uranium isotopes distinguish two geochemically distinct stages during the later Cambrian SPICE event. Earth. Planet. Sci. Lett. 401, 313–326. https://doi.org/10.1016/J.EPSL.2014.05.043.

Dang, D.H., Novotnik, B., Wang, W., Bastian Georg, R., Douglas Evans, R., 2016. Uranium isotope fractionation during adsorption, (co)precipitation, and biotic reduction. Environ. Sci. Technol. 50, 12695–12704. https://doi.org/10.1021/acs.est.6b01459.

Dang, D.H., Wang, W., Gibson, T.M., Kunzmann, M., Andersen, M.B., Halverson, G.P., Evans, R.D., 2022. Authigenic uranium isotopes of late Proterozoic black shale. Chem. Geol. 588, 120644. https://doi.org/10.1016/J.CHEMGEO.2021.120644.

Dewey, C., Sokaras, D., Kroll, T., Bargar, J.R., Fendorf, S., 2020. Calcium-uranyl-carbonato species kinetically limit U(VI) reduction by Fe(II) and lead to U(V)-bearing ferrihydrite. Environ. Sci. Technol. 54, 6021–6030. https://doi.org/10.1021/acs.est.9b05870.

Dickson, A.J., Idiz, E., Porcelli, D., Murphy, M.J., Celestino, R., Jenkyns, H.C., Poulton, S. W., Hesselbo, S.P., Hooker, J.N., Ruhl, M., van den Boorn, S.H.J.M., 2022. No effect of thermal maturity on the Mo, U, Cd, and Zn isotope compositions of Lower Jurassic organic-rich sediments. Geology. 50, 598–602. https://doi.org/10.1130/G49724.1.

Du, X., Boonchayaanant, B., Wu, W.M., Fendorf, S., Bargar, J., Criddle, C.S., 2011. Reduction of uranium(VI) by soluble iron(II) conforms with thermodynamic predictions. Environ. Sci. Technol. 45, 4718–4725. https://doi.org/10.1021/es2006012.

Easton, R.M., 2000. Metamorphism of the Canadian Shield, Ontario, Canada. II. Proterozoic metamorphic history. Can. Mineral. 38, 319–344. https://doi.org/10.2113/GSCANMIN.38.2.319.

Fralick, P., Planavsky, N., Burton, J., Jarvis, I., Addison, W.D., Barrett, T.J., Brumpton, G. R., 2017. Geochemistry of Paleoproterozoic Gunflint Formation carbonate: Implications for hydrosphere-atmosphere evolution. Precambrian. Res. 290, 126–146. https://doi.org/10.1016/J.PRECAMRES.2016.12.014.

Fralick, P.W., Davis, D.W., Kissin, S.A., 2002. The age of the Gunflint Formation, Ontario, Canada: single zircon U-Pb age determinations from reworked volcanic ash. Can. J. Earth. Sci. 39, 1085–1091. https://doi.org/10.1139/e02-028.

Gilleaudeau, G.J., Chen, X., Romaniello, S.J., Akam, S.A., Wittkop, C., Katsev, S., Anbar, A.D., Swanner, E.D., 2025. Uranium isotope systematics of a low-productivity ferruginous ocean analog: implications for the uranium isotope record of early Earth. Geochim. Cosmochim. Acta 392, 195–206. https://doi.org/10.1016/J.GCA.2025.01.011.

Gilleaudeau, G.J., Romaniello, S.J., Luo, G., Kaufman, A.J., Zhang, F., Klaebe, R.M., Kah, L.C., Azmy, K., Bartley, J.K., Zheng, W., Knoll, A.H., Anbar, A.D., 2019. Uranium isotope evidence for limited euxinia in mid-Proterozoic oceans. Earth. Planet. Sci. Lett. 521, 150–157. https://doi.org/10.1016/J.EPSL.2019.06.012.

Guilbaud, R., Poulton, S.W., Thompson, J., Husband, K.F., Zhu, M., Zhou, Y., Shields, G. A., Lenton, T.M., 2020. Phosphorus-limited conditions in the early Neoproterozoic ocean maintained low levels of atmospheric oxygen. Nat. Geosci. 2020 13, 296–301. https://doi.org/10.1038/s41561-020-0548-7, 4 13.

Hemming, S.R., McLennan, S.M., Hanson, G.N., 1995. Geochemical and Nd/Pb isotopic evidence for the provenance of the early Proterozoic Virginia Formation, Minnesota. Implications for the tectonic setting of the Animikie Basin. J. Geol. 103, 147–168. https://doi.org/10.1086/629733.

Holmden, C., Amini, M., Francois, R., 2015. Uranium isotope fractionation in Saanich Inlet: a modern analog study of a paleoredox tracer. Geochim. Cosmochim. Acta 153, 202–215. https://doi.org/10.1016/J.GCA.2014.11.012.

Johnston, D.T., Poulton, S.W., Fralick, P.W., Wing, B.A., Canfield, D.E., Farquhar, J., 2006. Evolution of the oceanic sulfur cycle at the end of the Paleoproterozoic. Geochim. Cosmochim. Acta 70, 5723–5739. https://doi.org/10.1016/j.gca.2006.08.001.

Kendall, B., Gordon, G.W., Poulton, S.W., Anbar, A.D., 2011. Molybdenum isotope constraints on the extent of late Paleoproterozoic ocean euxinia. Earth. Planet. Sci. Lett. 307, 450–460. https://doi.org/10.1016/j.epsl.2011.05.019.

Kipp, M.A., Li, H., Ellwood, M.J., John, S.G., Middag, R., Adkins, J.F., Tissot, F.L.H., 2022. 238U, 235U and 234U in seawater and deep-sea corals: a high-precision reappraisal. Geochim. Cosmochim. Acta 336, 231–248. https://doi.org/10.1016/J.GCA.2022.09.018.

Kipp, M.A., Tissot, F.L.H., 2022. Inverse methods for consistent quantification of seafloor anoxia using uranium isotope data from marine sediments. Earth. Planet. Sci. Lett. 577, 117240. https://doi.org/10.1016/J.EPSL.2021.117240.

Krogh, T.E., Davis, D.W., Corfu, F., 1984. Precise U-Pb zircon and baddeleyite ages for the Sudbury Area. In: Pye, E.G., Naldrett, A.J., Giblin, P.E. (Eds.), The Geology and Ore Deposits of the Sudbury Structure. Ontario Geological Survey, pp. 431–446.

Kulenguski, J.T., Gilleaudeau, G.J., Kaufman, A.J., Kipp, M.A., Tissot, F.L.H., Goepfert, T. J., Pitts, A.D., Pierantoni, P., Evans, M.N., Elrick, M., 2023. Carbonate uranium isotopes across Cretaceous OAE 2 in southern Mexico: new constraints on the global spread of marine anoxia and organic carbon burial. Palaeogeogr. Palaeoclimatol. Palaeoecol. 628, 111756. https://doi.org/10.1016/J.PALAEO.2023.111756.

Laakso, T.A., Schrag, D.P., 2014. Regulation of atmospheric oxygen during the Proterozoic. Earth. Planet. Sci. Lett. 388, 81–91. https://doi.org/10.1016/J.EPSL.2013.11.049.

Labotka, T.C., Papike, J.J., Vaniman, D.T., 1981. Petrology of contact metamorphosed argillite from the Rove Formation, Gunflint Trail, Minnesota. Am. Mineral. 66, 70–86.

Lau, K.V., Hancock, L.G., Severmann, S., Kuzminov, A., Cole, D.B., Behl, R.J., Planavsky, N.J., Lyons, T.W., 2022. Variable local basin hydrography and productivity control the uranium isotope paleoredox proxy in anoxic black shales. Geochim. Cosmochim. Acta 317, 433–456. https://doi.org/10.1016/J.GCA.2021.10.011.

Lau, K.V., Lyons, T.W., Maher, K., 2020. Uranium reduction and isotopic fractionation in reducing sediments: insights from reactive transport modeling. Geochim. Cosmochim. Acta 287, 65–92. https://doi.org/10.1016/j.gca.2020.01.021.

Liu, C., Gorby, Y.A., Zachara, J.M., Fredrickson, J.K., Brown, C.F., 2002. Reduction kinetics of Fe(III), Co(III), U(VI), Cr(VI), and Tc(VII) in cultures of dissimilatory metal-reducing bacteria. Biotechnol. Bioeng. 80, 637–649. https://doi.org/10.1002/BIT.10430.

Lu, X., Dahl, T.W., Zheng, W., Wang, S., Kendall, B., 2020. Estimating ancient seawater isotope compositions and global ocean redox conditions by coupling the molybdenum and uranium isotope systems of euxinic organic-rich mudrocks. Geochim. Cosmochim. Acta 290, 76–103.

Lu, X., Edwards, C.T., Kendall, B., 2023. No evidence for expansion of global ocean euxinia during the base Stairsian mass extinction event (Tremadocian, Early Ordovician). Geochim. Cosmochim. Acta 341, 116–131. https://doi.org/10.1016/J.GCA.2022.11.028.

Lucente, M.E., Morey, G.B., 1983. Stratigraphy and sedimentology of the lower proterozoic Virginia formation, Northern Minnesota. Minnesota Geol. Surv. Rep. Investig. 28.

Mänd, K., Lalonde, S.V., Robbins, L.J., Thoby, M., Paiste, K., Kreitsmann, T., Paiste, P., Reinhard, C.T., Romashkin, A.E., Planavsky, N.J., Kirsimäe, K., Lepland, A., Konhauser, K.O., 2020. Palaeoproterozoic oxygenated oceans following the Lomagundi–Jatuli Event. Nat. Geosci. 2020 13, 302–306. https://doi.org/10.1038/s41561-020-0558-5, 4 13.

Maric, M., 2006. Sedimentology and Sequence Stratigraphy of the Paleoproterozoic Rove and Virginia Formations, Southwest Superior Province. Lakehead University, Thunder Bay, Ontario. MSc Thesis.

Marshall, M.J., Beliaev, A.S., Dohnalkova, A.C., Kennedy, D.W., Shi, L., Wang, Z., Boyanov, M.I., Lai, B., Kemner, K.M., McLean, J.S., Reed, S.B., Culley, D.E., Bailey, V.L., Simonson, C.J., Saffarini, D.A., Romine, M.F., Zachara, J.M., Fredrickson, J.K., 2006. c-Type Cytochrome-Dependent Formation of U(IV) Nanoparticles by Shewanella oneidensis. PLoS. Biol. 4, e268. https://doi.org/10.1371/JOURNAL.PBIO.0040268.

Mclennan, S.M., 2001. Relationships between the trace element composition of sedimentary rocks and upper continental crust. Geochem., Geophys., Geosyst. 2.

Morford, J.L., Emerson, S., 1999. The geochemistry of redox sensitive trace metals in sediments. Geochim. Cosmochim. Acta 63, 1735–1750. https://doi.org/10.1016/S0016-7037(99)00126-X.

Ojakangas, R.W., Morey, G.B., Southwick, D.L., 2001. Paleoproterozoic basin development and sedimentation in the Lake Superior region. North America. Sediment. Geol. 319–341. https://doi.org/10.1016/S0037-0738(01)00081-1, 141–142.

Partin, C.A., Bekker, A., Planavsky, N.J., Scott, C.T., Gill, B.C., Li, C., Podkovyrov, V., Maslov, A., Konhauser, K.O., Lalonde, S.V., Love, G.D., Poulton, S.W., Lyons, T.W., 2013. Large-scale fluctuations in Precambrian atmospheric and oceanic oxygen levels from the record of U in shales. Earth. Planet. Sci. Lett. 284–293. https://doi.org/10.1016/j.epsl.2013.03.031, 369–370.

Pizarro-Koch, M., Pizarro, O., Dewitte, B., Montes, I., Paulmier, A., Garçon, V., Sepulveda, H.H., Corredor-Acosta, A., Aguirre, C., Ramos, M., 2023. On the interpretation of changes in the subtropical oxygen minimum zone volume off Chile during two La Niña events (2001 and 2007). Front. Mar. Sci. 10, 1155932. https://doi.org/10.3389/FMARS.2023.1155932.

Poulton, S.W., Fralick, P.W., Canfield, D.E., 2010. Spatial variability in oceanic redox structure 1.8 billion years ago. Nat. Geosci. 3, 486–490. https://doi.org/10.1038/ngeo889.

Poulton, S.W., Fralick, P.W., Canfield, D.E., 2004. The transition to a sulphidic ocean ~1.84 billion years ago. Nature 431, 173–177. https://doi.org/10.1038/nature02912.

Pufahl, P.K., Fralick, P.W., 2004. Depositional controls on Palaeoproterozoic iron formation accumulation, Gogebic Range, Lake Superior region, USA. Sedimentology 51, 791–808. https://doi.org/10.1111/J.1365-3091.2004.00651.X.

Reinhard, C.T., Planavsky, N.J., Robbins, L.J., Partin, C.A., Gill, B.C., Lalonde, S.V., Bekker, A., Konhauser, K.O., Lyons, T.W., 2013. Proterozoic ocean redox and biogeochemical stasis. Proc. Natl. Acad. Sci. 110, 5357–5362. https://doi.org/10.1073/pnas.1208622110.

Ripley, E.M., Park, Y.R., Lambert, D.D., Frick, L.R., 2001. Re-Os isotopic variations in carbonaceous pelites hosting the Duluth Complex: implications for metamorphic and metasomatic processes associated with mafic magma chambers. Geochim. Cosmochim. Acta 65, 2965–2978. https://doi.org/10.1016/S0016-7037(01)00635-4.

Rolison, J.M., Stirling, C.H., Middag, R., Rijkenberg, M.J.A., 2017. Uranium stable isotope fractionation in the Black Sea: modern calibration of the 238U/235U paleo-redox proxy. Geochim. Cosmochim. Acta 203, 69–88. https://doi.org/10.1016/j.gca.2016.12.014.

Romaniello, S.J., Herrmann, A.D., Anbar, A.D., 2013. Uranium concentrations and 238U/235U isotope ratios in modern carbonates from the Bahamas: Assessing a novel paleoredox proxy. Chem. Geol. 362, 305–316. https://doi.org/10.1016/j.chemgeo.2013.10.002.

Rutledge, R.L., Gilleaudeau, G.J., Remírez, M.N., Kaufman, A.J., Lyons, T.W., Bates, S., Algeo, T., 2024. Productivity and organic carbon loading control uranium isotope behavior in ancient reducing settings: implications for the paleoredox proxy. Geochim. Cosmochim. Acta. https://doi.org/10.1016/j.gca.2024.01.007.

Scott, C., Lyons, T.W., Bekker, A., Shen, Y., Poulton, S.W., Chu, X., Anbar, A.D., 2008. Tracing the stepwise oxygenation of the Proterozoic ocean. Nature 452, 456–459. https://doi.org/10.1038/nature06811.

Sheen, A.I., Kendall, B., Reinhard, C.T., Creaser, R.A., Lyons, T.W., Bekker, A., Poulton, S. W., Anbar, A.D., 2018. A model for the oceanic mass balance of rhenium and

implications for the extent of Proterozoic ocean anoxia. Geochim. Cosmochim. Acta 227, 75–95. https://doi.org/10.1016/j.gca.2018.01.036.
Shiel, A.E., Johnson, T.M., Lundstrom, C.C., Laubach, P.G., Long, P.E., Williams, K.H., 2016. Reactive transport of uranium in a groundwater bioreduction study: insights from high-temporal resolution 238U/235U data. Geochim. Cosmochim. Acta 187, 218–236. https://doi.org/10.1016/J.GCA.2016.05.020.
Stockey, R.G., Cole, D.B., Planavsky, N.J., Loydell, D.K., Frýda, J., Sperling, E.A., 2020. Persistent global marine euxinia in the early Silurian. Nat. Commun. 2020 11, 1–10. https://doi.org/10.1038/s41467-020-15400-y, 1 11.
Stylo, M., Neubert, N., Wang, Y., Monga, N., Romaniello, S.J., Weyer, S., Bernier-Latmani, R., 2015. Uranium isotopes fingerprint biotic reduction. Proc. Natl. Acad. Sci. 112, 5619–5624. https://doi.org/10.1073/pnas.1421841112.
Tissot, F.L.H., Dauphas, N., 2015. Uranium isotopic compositions of the crust and ocean: age corrections, U budget and global extent of modern anoxia. Geochim. Cosmochim. Acta 167, 113–143. https://doi.org/10.1016/J.GCA.2015.06.034.
Todd, J.F., Elsinger, R.J., Moore, W.S., 1988. The distributions of uranium, radium and thorium isotopes in two anoxic fjords: framvaren Fjord (Norway) and Saanich Inlet (British Columbia). Mar. Chem. 23, 393–415. https://doi.org/10.1016/0304-4203(88)90107-7.
Wang, X., Johnson, T.M., Lundstrom, C.C., 2015. Isotope fractionation during oxidation of tetravalent uranium by dissolved oxygen. Geochim. Cosmochim. Acta 150, 160–170. https://doi.org/10.1016/J.GCA.2014.12.007.
Wang, X., Planavsky, N.J., Hofmann, A., Saupe, E.E., De Corte, B.P., Philippot, P., LaLonde, S.V., Jemison, N.E., Zou, H., Ossa, F.O., Rybacki, K., Alfimova, N., Larson, M.J., Tsikos, H., Fralick, P.W., Johnson, T.M., Knudsen, A.C., Reinhard, C.T., Konhauser, K.O., 2018. A Mesoarchean shift in uranium isotope systematics. Geochim. Cosmochim. Acta 238, 438–452. https://doi.org/10.1016/J.GCA.2018.07.024.
Wang, X., Planavsky, N.J., Reinhard, C.T., Hein, J.R., Johnson, T.M., 2016. A Cenozoic seawater redox record derived from 238U/235U in ferromanganese crusts. Am. J. Sci. 316, 64–83. https://doi.org/10.2475/01.2016.02.
Weyer, S., Anbar, A.D., Gerdes, A., Gordon, G.W., Algeo, T.J., Boyle, E.A., 2008. Natural fractionation of 238U/235U. Geochim. Cosmochim. Acta 72, 345–359. https://doi.org/10.1016/J.GCA.2007.11.012.
Yang, S., Kendall, B., Lu, X., Zhang, F., Zheng, W., 2017. Uranium isotope compositions of mid-Proterozoic black shales: evidence for an episode of increased ocean oxygenation at 1.36 Ga and evaluation of the effect of post-depositional hydrothermal fluid flow. Precambrian. Res. 298, 187–201. https://doi.org/10.1016/J.PRECAMRES.2017.06.016.
Yang, S., Lu, X., Chen, X., Zheng, W., Owens, J.D., Young, S.A., Kendall, B., 2023. Uranium and molybdenum isotope evidence for globally extensive marine euxinia on continental margins and in epicontinental seas during the Devonian-Carboniferous Hangenberg crisis. Geochim. Cosmochim. Acta 352, 133–156. https://doi.org/10.1016/J.GCA.2023.04.027.
Zhang, F., Stockey, R.G., Xiao, S., Shen, S., Dahl, T.W., Wei, G.-Y., Cao, M., Li, Z., Kang, J., Cui, Y., Anbar, A.D., Planavsky, N.J., 2022. Uranium isotope evidence for extensive shallow water anoxia in the early Tonian oceans. Earth. Planet. Sci. Lett. 583, 117437. https://doi.org/10.1016/j.epsl.2022.117437.
Zhang, S., Li, Z.X., Evans, D.A.D., Wu, H., Li, H., Dong, J., 2012. Pre-Rodinia supercontinent Nuna shaping up: a global synthesis with new paleomagnetic results from North China. Earth. Planet. Sci. Lett. 145–155, 353–354.